Elastic depolarization and polarization transfer in CN (A2Π, v = 4) + Ar collisions

Iain Ballingall, Michael F Rutherford, Kenneth Mckendrick, Matthew Lawrence Costen

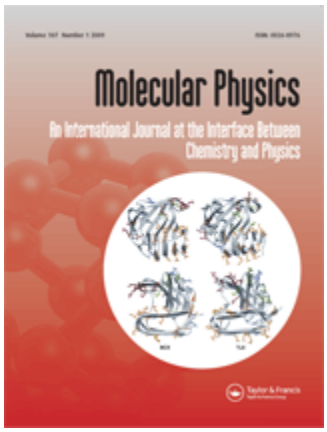

Elastic depolarization and polarization transfer in CN ($A^2\Pi$, v = 4) + Ar collisions

Journal:	*Molecular Physics*
Manuscript ID:	TMPH-2009-0330
Manuscript Type:	Special Issue Paper - In honour of Prof Richard Zare
Date Submitted by the Author:	20-Oct-2009
Complete List of Authors:	Ballingall, Iain; Heriot-Watt University, Engineering and Physical Sciences Rutherford, Michael; Heriot-Watt University, Engineering and Physical Sciences McKendrick, Kenneth; Heriot-Watt University, Engineering and Physical Sciences Costen, Matthew; Heriot-Watt University, Engineering and Physical Sciences
Keywords:	alignment, polarization, inelastic collisions, rotational energy transfer, rate constant

Elastic depolarization and polarization transfer in CN ($A^2\Pi$, $v = 4$) + Ar collisions

Iain Ballingall, Michael F. Rutherford, Kenneth G. McKendrick and Matthew L. Costen

School of Engineering and Physical Sciences, Heriot-Watt University, Edinburgh, U.K.

Dr M. L. Costen, School of Engineering and Physical Sciences, William Perkin Building, Heriot-Watt University, Edinburgh, EH14 4AS, U.K.
Email: m.l.costen@hw.ac.uk

(Received xx xxxxx 2009; final version received xx xxxxx 2009)

Rate constants for collisional loss and transfer of population and rotational angular momentum alignment have been determined for the CN($A^2\Pi$, $v = 4$) + Ar system. Aligned samples of CN($A^2\Pi$, $v = 4$, F_1, $j = 1.5 – 23.5$ e) were prepared by optical pumping on the A-X(4,0) band. Their evolution was observed using Doppler-resolved Frequency-Modulated Spectroscopy in stimulated emission on the A-X(4,2) band. State-resolved total population removal rate constants, and state-to-state rotational energy transfer (RET) rate constants, are found to be in excellent agreement with previous experimental measurements and theoretical predictions for the $v = 3$ level. Rapid elastic depolarization of rotational alignment was observed for $j = 1.5 – 6.5$, with an average rate constant of 1.1×10^{-10} cm^3 s^{-1}. This declines with increasing j, reaching zero within experimental error for $j = 23.5$. The polarization transfer efficiency of the initially created alignment in state-to-state RET was also determined for the selected initial state $j = 6.5$, F_1, e. Substantial depolarization of the alignment was observed for small Δj transitions. Alignment transfer efficiencies ranged from 0.55 ± 0.06 for $\Delta j = -1$, to 0.32 ± 0.08 for $\Delta j = +3$. These measurements are discussed with reference to recent experimental and theoretical advances on collisional depolarization of related open-shell species. We suggest that the surprisingly efficient collisional depolarization observed may be the result of the multiple potential energy surfaces involved in this system.

Keywords: alignment, polarization, frequency-modulated, rate constant, rotational energy transfer, CN, cyanogen radical, argon, vector correlations, inelastic collisions

1. Introduction

The transfer of energy between molecules in collisions is a fundamental process that is important in a wide range of gas-phase environments, such as combustion, plasmas, planetary atmospheres and the burgeoning field of ultra-cold matter.[1-4] As such, inelastic collisions have been the focus of a wide range of experimental and theoretical studies. Many of these have centred on the amount of energy transferred, a *scalar* quantity, by determining quantum state-to-state resolved population transfer

cross-sections or rate constants. A smaller proportion of theoretical and experimental studies have concentrated instead on the *vector* properties of the collision.[5,6] These are a more sensitive probe of the forces determining the outcome of the collision process than the scalar population information. The best known of these is probably the correlation between pre- and post-collision velocities, the differential cross-section or ($\boldsymbol{k}$-$\boldsymbol{k}'$) correlation. There have been a considerable number of crossed-molecular beam studies of rotational energy transfer (RET) in diatomic+atom or diatomic+diatomic collisions. The most sophisticated of these have extended to studying the plane of product rotation relative to the scattering plane, a ($\boldsymbol{k}$-$\boldsymbol{k}'$-$\boldsymbol{j}'$) correlation.[7,8] These have been shown to be very sensitive to the potential energy surface (PES) for the interaction.

A different experimental approach to vector studies of inelastic collisions is to use optical pumping to prepare an initial *anisotropic* distribution of $\boldsymbol{j}$ and observe its evolution, a ($\boldsymbol{j}$-$\boldsymbol{j}'$) correlation. This is usually performed in an optical-optical double resonance (OODR) experiment, where a polarized laser pulse generates either an orientation (a preference to rotate either clockwise or anti-clockwise), or an alignment (a preference for a particular plane of rotation).[9] Another polarized beam is then used to probe this orientation or alignment and its collisional evolution. When this is performed in a spatially isotropic collision environment, such as a thermalized bath of gas, then the orientation and alignment must ultimately be destroyed.[10] The experiments we report here are of this type. We can distinguish two separate types of ($\boldsymbol{j}$-$\boldsymbol{j}'$) correlation measurement. The first is the *loss* of polarization prepared in the initial level, through collisions that change the direction of $\boldsymbol{j}$ but not the magnitude. These we term *elastic depolarizing* collisions. The second is the *retention* of the initial

polarization in the course of population transfer to other quantum states, or *polarization transfer*.

Influential early experimental work, mainly on collisions of closed shell species with rare gas colliders, indicated that initially prepared polarizations were strongly conserved in both elastic and inelastic collisions.[5,11,12] Dynamical models of rigid ellipsoid – rigid sphere collisions give strong theoretical support to these observations.[13] However, many molecules of interest in environments such as combustion and the atmosphere are not well described as rigid ellipsoids. Open-shell molecules with non-zero orbital angular momentum, for example $^2\Pi$ states, require multiple PESs to describe their interactions even with the rare gases. In general, scattering theory predicts that conservation of polarization is not always expected to be the case for these systems.[14]

Recent experiments and scattering calculations have begun to show how significant depolarization can be in both elastic and inelastic collisions. A particular focus of these studies has been the OH radical, in both the $X^2\Pi$ and $A^2\Sigma^+$ states. Experiments have used various techniques under both controlled collision conditions[15-26] and in atmospheric pressure flames.[27-31] We have exploited Polarization Spectroscopy, a 3rd-order non-linear spectroscopic method,[16,32] to measure rate constants for elastic depolarization of both orientation and alignment of OH($X^2\Pi$ or $A^2\Sigma^+$) in collisions with rare gases and simple molecular colliders.[17,19-23,33] Comparison with full quantum scattering calculations on accurate *ab-initio* PESs has helped to unravel the influence of different parts of the PES on RET and elastic depolarization. Brouard and co-workers have used an independent technique, Zeeman quantum beat spectroscopy, to study elastic and inelastic depolarization in the OH(A)-Ar system,[23-25,34] and most recently NO($A^2\Sigma^+$)-Ar/He.[35] For OH(A), excellent

agreement is found between the two different experimental approaches, and with quasi-classical scattering calculations. This experimental work has stimulated corresponding theoretical advances. Extension of quantum scattering calculations to the prediction of elastic depolarization has enhanced the insight into the roles of different parts of the multiple PESs involved on competing elastic and inelastic processes.[36-38]

There are fewer more recent experimental studies of other species. Notable exceptions are the work of Rudert *et al.*, who studied elastic depolarization and polarization transfer of both orientation and alignment in C_2H_2 self-collisions,[39-41] and the measurement of alignment transfer in self-collisions of N_2 by Sitz and Farrow.[42,43] Further discussion of these experiments is deferred until later in this paper, but we note that these systems differ in being closed shell and therefore proceeding on single PESs. On the other hand, the added complexity of both partners being molecular presents hard theoretical challenges. We therefore consider it useful to extend collisional depolarization and transfer measurements to a system which is kinematically different to OH, but which retains the open-shell, $\Lambda \neq 0$, electronic structure, and for which quantum scattering calculations may in principle be relatively straightforwardly performed.

The specific focus of this work is therefore the CN radical in its $A^2\Pi$ first excited state. CN has become one of the prototype systems for state-resolved energy transfer, owing to its experimental convenience, and for collisions with noble gas atoms, its theoretical tractability.[44-52] Dagdigian, Alexander and co-workers have performed extensive measurements of RET with Ar and He in the $A^2\Pi(v = 3)$ state, which they have interpreted through quantum scattering calculations on accurate *ab-initio* PESs. In the case of CN, four PESs are required to describe the scattering

dynamics, two for scattering within the $A^2\Pi$ state, V_{sum} and V_{diff}, one for scattering within the $X^2\Sigma^+$ state, V_Σ, and one that describes the coupling between the Σ and $\Pi(A')$ states, V_1. Much of this work has been on the collisions of highly rotationally excited CN with Ar and He.[53-56] Importantly for the current study, RET with Ar at low-j was also studied, where good agreement was observed with theory for the relative state-to-state population transfer propensities.[57] Subsequent experimental and theoretical studies of the spectroscopy and predissociation dynamics of CN-Ar van der Waals complexes suggest that the PESs reported in ref. [57] understate the attractive forces in the system.[50,52] Specifically, although the anisotropy of the V_{sum} and V_{diff} PESs in the attractive regions was found to be accurate, scaling by a factor of 1.76 was required to match the observed dissociation energy of CN(A)-Ar, resulting in an amended V_{sum} well depth of D_e = 137.8 cm^{-1}.[52] Similarly, new *ab-initio* calculations supporting the spectroscopic measurements predict a substantially deeper attractive minimum for the V_Σ PES of D_e = 139 cm^{-1}.[50]

Despite this work on the *scalar* properties of RET in CN, there have been very few studies of the *vector* properties. The sole example is our own earlier work, where we have measured differential cross-sections for RET within the $A^2\Pi(v = 4)$ manifold.[58,59] These experiments exploited the 'photo-loc' technique, pumping a photolytically generated anisotropic velocity distribution to a selected rovibronic and Λ-doublet defined state, and probing the state-resolved product velocity distribution. The method relies on high velocity resolution in the probe step, achieved using frequency-modulated spectroscopy (FMS) with narrow-band continuous wave (cw) diode lasers.[60] In this paper, we adapt this technique, allowing the photolytically generated anisotropic velocity and angular momentum distributions to thermalize, before preparing an aligned sample in a selected $A^2\Pi(v = 4)$ rotational state. The

evolution of the prepared population and alignment in collisions with Ar is then observed using FMS. We report rate constants for the removal of the initially prepared population and state-to-state population transfer. We also report alignment depolarization rate constants for the initially prepared levels and state-to-state alignment transfer rate propensities for a selected initial level. We discuss the results in light of the literature PESs and recent studies of related systems.

2. Experimental

The experimental apparatus has been explained in detail before, so only the essential details are described here.[58,59,61] In essence, the experiments used three separate laser systems: a pulsed photolysis beam to generate CN(X) from ICN; a pulsed pump beam to excite a unique spectroscopic level in CN($A^2\Pi$, $v = 4$); and a cw probe beam to monitor the time evolution of either the prepared level, or a collisional product level. The experiments were performed in a custom-built vacuum chamber, evacuated by a diffusion pump. The chamber contained two pairs of plane mirrors arranged in a square. The photolysis beam was reflected in a multi-pass geometry between one pair (highly reflective (HR) at 266 nm) and the pump and probe beam were similarly reflected between the other pair of mirrors (HR 600-900 nm). The pump beam and the probe beam counterpropagated, orthogonal to the photolysis beam.

Approximately 15 mTorr of ICN was admitted to the chamber in a slow flow. The collider gas, Ar (research grade, BOC), was added via a mass flow controller (MKS Instruments, 100 s.c.c.m.) to attain the desired total pressure (100 - 1000 mTorr), monitored by a capacitance manometer (MKS Instruments).

The ICN was photolyzed at 266 nm by a Nd:YAG laser (Continuum Surelite III -10) to produce CN radicals in the $X^2\Sigma^+$ ($v = 0$) state. Initially these nascent CN photofragments have a near mono-energetic speed distribution in a wide range of

rotational states.[62] In the current experiments the introduction of a delay of ≈ 5 μs after the photolysis pulse ensured the thermalization of the nascent translational and rotational angular momentum anisotropy.[61] The CN was then pumped from a range of $X^2\Sigma^+$ ($v = 0, j, f_1$) levels to specific $A^2\Pi$ ($v = 4, j, F_1, e$) levels using a Nd:YAG pumped dye laser (Spectron, SL803/SL4000) tuned to selected transitions of the R_1 branch of the $A^2\Pi$-$X^2\Sigma^+$ (4,0) band around 620 nm. Care was taken to avoid lines subject to accidental spectroscopic overlap. The pump beam passed through a photo-elastic modulator (PEM-80, Hinds Inc.) and by controlling the timings of the photolysis and pump lasers with a delay generator (Stanford Research Systems, DG535) the pump polarization was switched between horizontal and vertical in the laboratory. The pump laser fluence was ≈ 60 mJ cm^{-2}. This represented the optimum compromise between a higher prepared population and reduced alignment due to increasing saturation of the transition at higher pump fluence.

The CN $A^2\Pi$ state molecules were probed by FMS in stimulated emission, using an external cavity tuneable diode laser (Sacher GmbH, TEC500) on the R_1 and Q_1+$^QR_{12}$ branches of the $A^2\Pi$-$X^2\Sigma^+$(4,2) band. Note that we use the spectroscopic notation for *absorption* throughout this paper, for both the pump and probe steps. The probe beam was vertically polarized by a calcite polarizer, and then frequency modulated at 400 MHz by a broadband phase modulator (Quantum Technology, TWAP-10), driven by a frequency generator (Thurlby Thandar, TGR1040). After multi-passing through the chamber the probe beam was directed onto a 1 GHz photo-receiver (New Focus, 1601FS-AC). The 400 MHz output signal was passed to an I & Q demodulator (Pulsar Microwave, ID-10-412) which provided transient in-phase (I) and quadrature (Q) signals. A digital storage oscilloscope (LeCroy, LT342) averaged the I & Q signals independently for a preset number (typically 30) of combined

photolysis and pump laser shots at each probe laser wavelength. The probe laser was scanned across the transition of interest in 100 MHz increments. The $X^2\Sigma^+(v = 2)$ ground state has a small, but non-zero population from ICN photolysis,[63] which can contribute an absorption component to the probe signal. Background signals were therefore acquired in the absence of the pump laser (in practice, by firing it 1 μs before the photolysis laser). Thus at each probe wavelength step, four experimental timetraces were acquired sequentially, comprising pump-induced and background signals for both the horizontal and vertical pump polarizations. This resulted in four sets of three-dimensional arrays of both I & Q signals as a function of frequency and time. The spectral trace from a scanning Fabry-Perot interferometer monitoring the modulated diode beam was also recorded for each wavelength step, for the purposes of calibrating the frequency scale. All data acquisition was controlled by custom-written LABVIEW® software.

3. Data Analysis

3.1 Determiation of time-dependent population and alignment

In the absence of saturation, the linearly polarized pump beam preferentially pumps CN molecules in proportion to the components of their transition dipole moments parallel to the electric vector of the pump radiation. The upper state rotational angular momentum, $\boldsymbol{j}$, is therefore aligned.[9] As the ground-state $\boldsymbol{j}$ is isotropically distributed before pumping, the resulting excited state $\boldsymbol{j}$ distribution is cylindrically symmetric about the *pump* polarization. We can thus describe the prepared upper state in terms of a population, $A_0^{(0)}$ and a single rotational alignment moment of tensor rank $K = 2$, $A_0^{(2)}$. In practice, our experiments are performed in a saturated regime, which may result in alignment moments of higher tensor rank in the prepared distribution.

However, the linearly polarized FM probe is only sensitive to moments with K =0 and 2,[9,64] and in an isotropic environment collisions cannot mix moments of different tensor rank.[10] We can therefore still consider the prepared and probed distribution as described purely by $A_0^{(0)}$ and $A_0^{(2)}$.

The linearly polarized probe will have different relative sensitivities to $A_0^{(0)}$ and $A_0^{(2)}$ depending on both the relative linear polarizations of the pump and probe lasers and the spectroscopic branch used. We define our two geometries as parallel (||) and perpendicular ($\perp$), depending on the relative polarizations of the counter-propagating pump and probe beams. In contrast to our previous work on CN energy transfer,[58,59,61] the Doppler lineshapes here contain no useful information. For an isotropic velocity distribution such as that used in these experiments, all of the information is contained within the relative intensities, I, of the overall integrated lineshapes, and can be expressed as[65,66]

$$I_{\parallel} = \frac{CS}{3(2j+1)} A_0^{(0)}\left[1 + h^{(2)} A_0^{(2)}\right] \qquad (1)$$

$$I_{\perp} = \frac{CS}{3(2j+1)} A_0^{(0)}\left[1 - \frac{h^{(2)}}{2} A_0^{(2)}\right] \qquad (2)$$

Here S is the rotational linestrength and $h^{(2)}$ the rotational branch alignment sensitivity. Note that the relevant value of $h^{(2)}$ is that for the stimulated emission branch, e.g. the transition labelled as $R_1(5.5)$ in absorption has the alignment sensitivity of $P_1(6.5)$ in stimulated emission. C is a constant containing the experimental sensitivity to all other parameters, such as absolute number density, pathlength and detector sensitivity. As defined here, the alignment, $A_0^{(2)}$, has the conventional high-j limits of -1 and +2.[9]

Our experiments measure FM Doppler lineshapes, which may be transformed to conventional Doppler lineshapes by either a stepwise recursive, or numerical

integration-based, inversion procedure.[60] This may then be integrated to yield the total line intensity, as described in eqns 1 and 2 above. Figure 1 shows the result of this procedure for the $A^2\Pi$ ($v = 4$, $j = 2.5$, F_1, e) state, prepared by pumping the $R_1(1.5)$ transition of the A-X(4,0) band and probed on the same transition in the A-X(4,2) band. The intensities for the parallel and perpendicular geometries are displayed as a function of time after the pump pulse, at a total pressure of 200 mTorr. The signal for the parallel geometry is clearly larger than that for the perpendicular geometry, indicating that a rotational alignment has indeed been generated. The signals for the two geometries decay as collisions remove the initially prepared population, but crucially the curves converge before reaching zero intensity. This indicates that there must be a process destroying the alignment that is independent of population loss, i.e. an elastic depolarization process. We note at this point that in principle quantum beats from the coupling of the nuclear spin, $\boldsymbol{I}$, of the ^{14}N ($I = 1$) to $\boldsymbol{j}$ might be expected for this low-j state, as have been observed for aligned samples in the $X^2\Sigma^+$ state.[67] No such beats were observed in any of the low-j states probed. Although we know of no measurements of the hyperfine splittings in the $A^2\Pi(v = 4)$ level, they have been recently measured in the $v = 1$ level.[68] Assuming that the splittings are of similar magnitude in the two vibrational levels, they would give rise to nuclear hyperfine quantum beats with maximum frequencies ranging from ≈ 90 MHz for the lowest j studied here to ≈ 30 MHz at the highest j. Our experiment has a relatively slow response time of ~ 35 ns (10% - 90% signal) which results from the long optical path overlap (≈ 6 m), coupled with the ~ 15 ns pump laser pulsewidth. For essentially all of the states prepared here, the combined pump pathlength and pulsewidth will result in a sample that has an alignment determined by the time-averaged nuclear hyperfine depolarization (NHD). A further blurring of any residual beat amplitude will also

arise from the identical, counter-propagating, probe pathlength and consequent measurement time. We therefore treat all further measured alignments as subject to time-averaged NHD.[9]

In principle, as can be seen from inspection of eqns. 1 and 2, $I_{\parallel}$ and $I_{\perp}$ could be linearly combined to yield curves dependent on only the population and the alignment, respectively. In practice, this involves several stages of data processing (FM to 'normal' Doppler profile, integration and linear combination) that can introduce unwanted artifacts into the data, and propagate noise in an unpredictable fashion.[60,62]

We have instead chosen a numerically more robust approach, which is to fit our experimental data directly as FM Doppler lineshapes. The collected background FM I & Q data sets were subtracted from the equivalent pump data sets, and the resulting background-corrected I & Q data sets were rotated[69] to yield pure stimulated emission (SE) and dispersion (D) as a function of time and frequency. FM Doppler lineshapes for sequential 10 ns averages of the SE and D signals for each of the two geometries were constructed, with the wavelength axis linearized using the acquired monitor etalon traces. At each 10 ns time interval, this resulted in 4 FM Doppler profiles, consisting of SE and D for each geometry. Synthetic 'normal' Gaussian Doppler profiles (with integral areas given by equations 1 and 2), were generated from an assumed population and alignment, along with the corresponding dispersion lineshapes.[69] Both synthetic SE and D simulated lineshapes were then transformed to FM SE and D lineshapes and fitted simultaneously to the experimental data. The assumed population and alignment were iteratively varied to give the optimum least-squares fit between synthesis and experiment. Figure 2 gives an example of the quality of the fit at the peak of the prepared distribution, and illustrates the magnitude

of the dependence of the signal on geometry. The fitted population, $A_0^{(0)}$, and rotational alignment, $A_0^{(2)}$, were determined as a function of post-pump delay time for further kinetic analysis.

3.2 Kinetics of population and alignment decay

The kinetics of the decay of an initially prepared population and alignment have been described in detail in several recent publications.[34,36] We may therefore define a tensor rate, $\Gamma_{j\to j'}^{(K)}$, in terms of the microscopic rates for transfer from an initial state $\left|jm_j\right\rangle$ to some final state $\left|j'm_{j'}\right\rangle$ [34,36,70] (note that in what follows, Γ will be used to represent *rates* whilst, *k* will represent *rate constants*):

$$\Gamma_{j\to j'}^{(K)} = \sum_{m,m'} (-1)^{j-m-j'-m'} (2K+1) \begin{pmatrix} j' & j' & K \\ m' & -m' & 0 \end{pmatrix} \begin{pmatrix} j & j & K \\ m & -m & 0 \end{pmatrix} \Gamma_{jm\to j'm'} \qquad (3)$$

where the terms in brackets are 3-j symbols, *K* is the tensor rank order and $\Gamma_{jm\to j'm'}$ are the microscopic rates. When initial and final levels are the same, we define the *elastic* depolarization rate, $\Gamma_{jj}^{(K)}$, as the difference[36] of the totally elastic rate (i.e. $\Delta j = 0$, $\Delta m_j = 0$), $\Gamma_{j\to j}^{(0)}$, and the relevant tensor rate, $\Gamma_{j\to j}^{(K)}$ (which we note again refers to *retention* of polarization)

$$\Gamma_{jj}^{(K)} = \Gamma_{j\to j}^{(0)} - \Gamma_{j\to j}^{(K)} \qquad (4)$$

Considering a kinetic scheme within which we assume no significant transfer back from other rotational states populated by RET, but allow elastic depolarization, the time evolution of the tensor moments of the density matrix for the initial level, *j*, is given as;

$$\rho_0^{(K)}(j;t) = \rho_0^{(K)}(j;t=0) e^{-\Gamma_{j,tot}^{(K)} t} \qquad (5)$$

Here the decay rate, $\Gamma_{j,tot}^{(K)}$ is sum of the elastic depolarization rate, $\Gamma_{jj}^{(K)}$ and the total population removal rate, $\Gamma_{jj}^{(0)}$. The latter is simply the sum of the state-to-state removal rates out of that initial level to all unobserved final levels, j_x.

$$\Gamma_{j,tot}^{(K)} = \Gamma_{jj}^{(0)} + \Gamma_{jj}^{(K)} \qquad (6)$$

$$\Gamma_{jj}^{(0)} = \sum_{j_x} \Gamma_{j\to j_x}^{(0)} \qquad (7)$$

We note that in our independent related PS experiments on the OH radical,[16,23] the signal observed is a measurement of the bulk polarization of the sample, and therefore directly of the tensor moments of the density matrix. Hence $\Gamma_{j,tot}^{(K)}$ is identical to the PS removal rates, $\Gamma_{PS}^{(K)}$, defined in our previous work. The alignment measured in the current experiment, in contrast, is renormalized from the tensor moments by both a *j*-dependent factor, which has been previously defined in the literature of coherent photodissociation dynamics as *V(j)*,[64,71] and by the $K = 0$ tensor moment, i.e. the population.[72]

$$\begin{aligned} A_0^{(2)}(j;t) &= \left[\frac{(2j+3)(2j-1)}{5j(j+1)}\right]^{1/2} \frac{\rho_0^{(2)}(j;t)}{\rho_0^{(0)}(j;t)} \\ &= \left[\frac{1}{V(j)\sqrt{5}}\right] \frac{\rho_0^{(2)}(j;t)}{\rho_0^{(0)}(j;t)} \qquad (8), (9), (10) \\ &= A_0^{(2)}(j;t=0) e^{-\Gamma_{jj}^{(2)} t} \end{aligned}$$

Thus the measured alignment will exhibit single exponential decay with the rate $\Gamma_{jj}^{(2)}$. These tensor removal rates may then be related to the desired bimolecular tensor rate *constants*, $k_{jj}^{(K)}$.

$$\Gamma_{jj}^{(K)} = k_{jj,\text{int}}^{(K)} + k_{jj}^{(K)}[M] \qquad (11)$$

Here, [*M*] is the collider number density, and $k_{jj,\text{int}}^{(K)}$ is a tensor-dependent zero-pressure intercept rate, resulting from collisions with the precursor and non-collisional loss processes, such as 'fly-out' from the probed region.

3.3 Kinetics of population and alignment transfer

In principle, a full master equation model based on the tensor moment rate formalism could be developed for the population and alignment transfer. However, a simpler approach is to consider a three-level kinetic scheme, and restrict the subsequent data analysis to early times, where transfer via multiple collisions will be unimportant. The three-level scheme is defined as;

$$\begin{array}{l} j \xrightarrow{\Gamma^{(K)}_{j\to j'}} j' \xrightarrow{\Gamma^{(K)}_{j'\to j_x}} j_x \\ j \xrightarrow{\Gamma^{(K)}_{j\to j_x}} j_x \\ j \xrightarrow{\Gamma^{(K)}_{j\to j}} j \qquad j' \xrightarrow{\Gamma^{(K)}_{j'\to j'}} j' \end{array} \tag{12}$$

Here j is the initial level, j' is the probed product level and j_x represents all unobserved levels. Note that we include elastic depolarization of both the initial and the product levels. This scheme and the definition of the tensor rates may be used to derive the time evolution of the tensor moments of the product-state density matrix.

$$\frac{d\rho_0^{(K)}(j';t)}{dt} = \rho_0^{(K)}(j;t)\Gamma^{(K)}_{j\to j'} - \rho_0^{(K)}(j')\Gamma^{(K)}_{j',tot} \tag{13}$$

where we already know the time evolution of the initial-state density matrix from eqn 5. This is a standard kinetic problem which may be solved easily to give the time evolution of the product-state density matrix.

$$\rho_0^{(K)}(j';t) = \frac{\rho_0^{(K)}(j;t=0)\Gamma^{(K)}_{j\to j'}\left\{e^{-\Gamma^{(K)}_{j',tot}t} - e^{-\Gamma^{(K)}_{j,tot}t}\right\}}{\Gamma^{(K)}_{j,tot} - \Gamma^{(K)}_{j',tot}} \tag{14}$$

Considering the population, i.e. taking the tensor rank, $K = 0$, we find the expected standard result;

$$\rho_0^{(0)}(j';t) = \rho_0^{(0)}(j;t=0)\left[\frac{\Gamma^{(0)}_{j\to j'}}{\Gamma^{(0)}_{jj} - \Gamma^{(0)}_{j'j'}}\right]\left\{e^{-\Gamma^{(0)}_{j'j'}t} - e^{-\Gamma^{(0)}_{jj}t}\right\} \tag{15}$$

The transferred population will exhibit a rise and fall with rates determined by the total removal rates of the initial and product levels, and an overall magnitude

dependent on these rates, the initial population and the desired state-to-state rate, $\Gamma^{(0)}_{j\to j'}$.

The time dependence of the transferred alignment can then be found from eqn 14 with the tensor order $K = 2$, normalized by eqn 15, i.e. the population, and the previously described j-dependent factors (see eqns 8 and 9).

$$A_0^{(2)}(j';t) = A_0^{(2)}(j;t=0)\left[\frac{V(j)}{V(j')}\right]\left[\frac{\Gamma^{(2)}_{j\to j'}}{\Gamma^{(0)}_{j\to j'}}\right]\left[\frac{\Gamma^{(0)}_{jj}-\Gamma^{(0)}_{j'j'}}{\Gamma^{(2)}_{j,tot}-\Gamma^{(2)}_{j',tot}}\right]\left[\frac{e^{-\Gamma^{(2)}_{j',tot}t}-e^{-\Gamma^{(2)}_{j,tot}t}}{e^{-\Gamma^{(0)}_{j'j'}t}-e^{-\Gamma^{(0)}_{jj}t}}\right] \qquad (16)$$

In principle we have measured all of the rates in this expression in separate experiments, and so could extract the desired rate, $\Gamma^{(2)}_{j\to j'}$. However, inspection allows us to greatly simplify this expression. We have measured the elastic depolarization rates for a variety of the initial and final levels, and although there is a general decline with increasing j, there is no significant variation over the range of product j' probed here for our chosen initial level, within our experimental precision. Therefore assuming that the elastic alignment depolarization rates are the same in initial and final levels, $\Gamma^{(2)}_{jj} = \Gamma^{(2)}_{j'j'}$, and remembering that the total tensor depolarization rates are the sum of the population removal and elastic depolarization rates (eqn 6), we find;

$$A_0^{(2)}(j';t) = A_0^{(2)}(j;t=0)\left[\frac{V(j)}{V(j')}\right]\left[\frac{\Gamma^{(2)}_{j\to j'}}{\Gamma^{(0)}_{j\to j'}}\right]e^{-\Gamma^{(2)}_{jj}t} \qquad (17)$$

This implies that the transferred alignment in level j' should decay with a single exponential rate, from an initial magnitude that is defined by the prepared alignment in the initial level, j, and scaled by a j, j' dependent renormalization factor (which is very close to unity for all the states probed in these experiments), and the ratio of the tensor rate for alignment transfer to the population transfer rate. This ratio is the desired quantity in these experiments, and is equivalent to the multipole transfer efficiency defined by Orlikowski and Alexander[73], and the multipole transfer co-efficients of Brouard and co-workers.[34]

4. Results

4.1 Population and alignment decay of initially prepared states

The rate constants for total population loss and elastic depolarization were measured for selected initially prepared CN $A^2\Pi(v = 4, F_1, j, e)$ levels in the range $j = 1.5 – 23.5$, using the R_1 branch lines. The time dependences of $A_0^{(0)}$ and $A_0^{(2)}$ were determined as described above. Experiments were performed for typically six different total pressures in the range 100 - 1000 mTorr. Figure 3 shows example time-dependences for $A_0^{(0)}$ and $A_0^{(2)}$ for the $j = 2.5$ state at total pressures of 200 and 1000 mTorr. The solid lines are single exponential fits to the experimental results, based on the kinetic analysis for removal of the population (eqn 5 with $K = 0$) and alignment (eqn 10) of the initially prepared level in the previous section. The relatively large density of states (j, F_1/F_2, e/f) available for CN $A^2\Pi$ results in a small fractional population in any one rotational level upon complete thermalization, with this particular state having a fractional Boltzmann population of 1.27% at 295 K. The $A^2\Pi(v = 4)$ state also loses population through both radiation ($\tau_{rad} = 3.83 \pm 0.2$ μs)[74], and collisional transfer to vibrationally excited levels of the $X^2\Sigma^+$ state.[75] Thus we do not expect collisional back transfer into the initially prepared state to be a significant process, as confirmed by the excellent quality of fit to a single exponential decay. This justifies the kinetic analysis of the alignment used. The alignment created by the pump laser is initially negative, as expected for R-branch pumping on this perpendicular band.[9] It also decays exponentially with time, but with a finite rate. This clearly indicates that *elastic depolarizing* collisions ($\Delta j = 0$, $\Delta m_j \neq 0$) are significant on the timescale of RET. The first 70 ns was excluded from fits of both population and alignment, to ensure that periods during which the population and alignment were still being established were not sampled. At late times, where the population is small,

the alignment is numerically not well determined, resulting in large, unphysical, fluctuations. The range to which the alignment exponential decay was fitted was therefore truncated to exclude regions where the population had fallen to less than 10% of its peak value. As previously discussed, we do not observe nuclear hyperfine quantum beats in this $j = 2.5$ data, as the time response of the experiment is too slow. We instead measure a time-averaged depolarized alignment that is, for $j = 2.5$, 61% of that instantaneously created by the pump laser.[9] This averaged NHD has no effect on the measurement of the collisional rate of alignment decay.

The fitted decay rates for population, $\Gamma_{jj}^{(0)}$ and alignment, $\Gamma_{jj}^{(2)}$ were used to determine the 2nd-order rate constants for population loss, $k_{jj}^{(0)}$ and for the alignment elastic depolarization, $k_{jj}^{(2)}$, as defined in eqn 11. Figure 4 shows example 2nd-order plots for both population and alignment for $j = 2.5$ and $j = 13.5$. Clearly, $k_{jj}^{(0)}$ is larger than $k_{jj}^{(2)}$ for both rotational levels, while both $k_{jj}^{(0)}$ and $k_{jj}^{(2)}$ are significantly larger for $j = 2.5$ than for $j = 13.5$. The intercepts also vary. For both levels, the intercept for population, $k_{jj,\mathrm{int}}^{(0)}$, is larger than that for alignment, $k_{jj,\mathrm{int}}^{(2)}$, but both intercepts are smaller for larger j. This is a general trend observed from all of the second-order plots, with $k_{jj,\mathrm{int}}^{(0)}$ declining from ~ 1.5 x 10^6 s^{-1} for low-j to ~ 8 x 10^5 s^{-1} for the highest j observed here, whilst $k_{jj,\mathrm{int}}^{(2)}$ declines from ~ 5 x 10^5 s^{-1} to essentially zero at high-j. The intercept rate $k_{jj,\mathrm{int}}^{(0)}$ contains contributions from both collisions with the precursor ICN, and non-collisional processes, in particular 'fly-out' of the CN from the probed region, and to a lesser extent radiative losses (k_{rad} = 2.61 x 10^5 s^{-1}). In contrast, fly-out and radiative emission cannot contribute to $k_{jj,\mathrm{int}}^{(2)}$, which can only consist of contributions from processes which selectively depolarize the alignment. We

therefore believe that the major contribution to $k^{(2)}_{jj,\mathrm{int}}$ arises from collisional depolarization by the ICN precursor, which appears to be much more efficient for low-*j*. Consistent with this interpretation, efficient RET and collisional depolarization of low-*j* CN($X^2\Sigma^+$) by ICN has been previously observed in studies of nascent photolytic products,[67] suggested to arise as a result of dipole-dipole interactions.

The complete sets of measured rate constants are shown in figure 5 as a function of *j*. There is a clear and consistent decline in $k^{(0)}_{jj}$ with increasing *j*, from a low-*j* peak of ~ 4 x 10^{-10} cm^3 s^{-1}. There is also a clear decrease, although with more scatter, in $k^{(2)}_{jj}$, from ~ 1 x 10^{-10} cm^3 s^{-1} at low-*j* to essentially zero within measurement error at *j* = 23.5.

4.2 State-to-state population and alignment transfer

In this set of experiments, the total pressure was fixed at 400 mTorr (15 mTorr ICN + 385 mTorr Ar). The pump laser was tuned exclusively to the $R_1(5.5)$ transition of the A-X(4,2) band, preparing $A^2\Pi(v = 4, j = 6.5, F_1, e)$. Various product states of RET within the $A^2\Pi(v = 4, F_1)$ manifold were probed on a variety of R_1 and Q_1+$^QR_{12}$ branch lines, covering both positive and negative Δj and both Λ-doublets. In each set of experiments, the initially prepared level was probed before each set of product levels, providing a calibration of the initially prepared population and alignment. For the mixed Q_1+$^QR_{12}$ branch lines, noting that in SE, these probe the *same* $A^2\Pi$ state and terminate in different $X^2\Sigma^+$ spin-rotation states, the Doppler profiles were fit using sums of two Gaussian lineshapes, with relative intensities determined by the alignment sensitivity and rotational linestrengths. Figure 6 shows the FM Doppler profiles and fits for the $Q_1(9.5)$+$^QR_{12}(8.5)$ transition at a delay of 75 ns. The main $Q_1(9.5)$ line is noticeably larger for the perpendicular geometry (Fig. 6(b)) than for the

parallel geometry (Fig. 6(a)). This indicates a negative alignment, as the Q branch has an opposite (and approximately twice the magnitude) alignment sensitivity to that of the R branch. However, comparing this to Fig. 2 we see that the relative difference between polarisations is considerably smaller for this state which is a product of RET, indicating that the transferred alignment is smaller than that typically generated in the pump step. The kinetic traces resulting from this fitting procedure from the initially prepared and product levels, for both population and alignment, were then used to determine state-to-state population rate constants and alignment transfer efficiencies.

4.3 Population transfer

The rate equation for the transferred population derived in the previous section (eqn 15) was used to determine the state-to-state population transfer rate constants. The population at $t = 0$ of the initial level, j, and its loss rate, $\Gamma_{jj}^{(0)}$, were first found by fitting the kinetic traces for the initially prepared level (as in eqn 5 with $K = 0$). These were then used in a non-linear least squares fit to eqn. 15 to find the total loss rate of the product state, $\Gamma_{j'j'}^{(0)}$, and the state to state rate, $\Gamma_{j\to j'}^{(0)}$. Figure 7 shows the kinetic traces for the initially prepared level and three different product states, from data acquired in a single sequence of scans on the same day, together with their fits as just described. The state-to-state rates were then converted to rate constants, $k_{j\to j'}^{(0)}$ assuming a total pressure of 400 mTorr. These phenomenological rate constants include a contribution from the ICN precursor, which, on the basis of the maximum precursor contribution to the total removal rate constants, we estimate to be less than 15%. The resulting state-to-state rate constants for the product levels probed are displayed in figure 8.

4.4 Alignment transfer

The simplest method of determining the transferred alignment would be to take the average alignment during an early time window, when only single collisions may be expected to be significant. However, this clearly suffers from the disadvantage of low signal levels and therefore poor determination of the alignment. We hence adopted an alternative approach, fitting the transferred alignment kinetics, using a longer duration sample of the measured alignment.

From day-to-day, the magnitude of the prepared alignment varied with pump laser fluence and the pump-probe beam overlap, in the range $A_0^{(2)} = -0.28 \pm 0.07$. As described previously, the measured prepared alignment will have been reduced by NHD from that instantaneously created by the pump laser. The measured alignment, not a value corrected to remove the effect of NHD, is therefore the initial alignment available to undergo polarization transfer in these experiments. The decay of this initially prepared alignment was fit to a single exponential in the same fashion as in the depolarization studies, to extract $A_0^{(2)}$ ($j = 6.5$, e; $t = 0$). The product alignment was also fitted to a single exponential decay, as described by eqn 17 above, with the fitted delay range truncated to < 600 ns to minimize the influence of secondary collisions. Figure 9 shows examples of the initial alignment and two transferred alignment decays, together with their respective fits. The nuclear spin is expected to be a spectator in the collision, as observed in OH(A)+Ar collisions.[23,25,34] After collision, $\boldsymbol{I}$ will recouple to $\boldsymbol{j'}$, resulting in a reduction in the measured transferred alignment from time-averaged NHD. In principle, however, the nuclear spin is no longer isotropic, as the initial depolarization of $\boldsymbol{j}$ will have resulted in a corresponding (time-varying, with defined average) alignment of $\boldsymbol{I}$.[76] However, given the relative magnitudes of $\boldsymbol{j}$ and $\boldsymbol{I}$, the magnitude of the alignment stored in the nuclear spin is low for $j = 6.5$. We

calculate the time-averaged nuclear alignment generated to be only ≈ 1% of the initial rotational alignment for $j = 6.5$. In practice, therefore, we have corrected the measured product alignments of $\boldsymbol{j'}$ to reflect the alignment that would have been transferred in the absence of time-averaged NHD in the product state. The extrapolated $t = 0$ initial and product state alignments yield the desired ratio of the tensor alignment rate to the population rate.

$$\left[\frac{\Gamma^{(2)}_{j\to j'}}{\Gamma^{(0)}_{j\to j'}}\right] = \left[\frac{A^{(2)}_0(j';t=0)}{A^{(2)}_0(j;t=0)}\right]\left[\frac{V(j')}{V(j)}\right] \qquad (18)$$

To the extent that the collider-independent intercept rates for population and alignment transfer are negligible, this ratio of rates will also be the ratio of the state-to-state rate constants.

$$\left[\frac{\Gamma^{(2)}_{j\to j'}}{\Gamma^{(0)}_{j\to j'}}\right] = \left[\frac{k^{(2)}_{j\to j',\mathrm{int}} + k^{(2)}_{j\to j'}[M]}{k^{(0)}_{j\to j',\mathrm{int}} + k^{(0)}_{j\to j'}[M]}\right] \approx \left[\frac{k^{(2)}_{j\to j'}}{k^{(0)}_{j\to j'}}\right] \qquad (19)$$

Figure 10 shows the average of this ratio for multiple measurements taken on different days, for a variety of product states.

5. Discussion

5.1 Collisional removal of initially prepared population and alignment

We first consider the collisional removal of the initially prepared population and alignment. The total population removal rate constants shown in figure 5 vary from ≈ 4.0 x 10^{-10} cm^3 s^{-1} for low j to ≈ 2.6 x 10^{-10} cm^3 s^{-1} for $j = 23.5$. The gradual decline in the overall removal rate with increasing j is familiar, almost universal, behaviour. It is consistent with the increasing energy gaps between adjacent rotational levels, which reach ≈ 80 cm^{-1} at $j = 23.5$. There are, of course, open channels with smaller energy gaps to the other Λ-doublet and spin-orbit states. However, their contribution to the overall rate constant is not large enough to overcome the generally expected, energy-gap dominated trend. The closest available literature comparison is with the

experiments and theory of Alexander *et al.*[57] They measured and predicted $k_{jj}^{(0)}$ for one of the rotational levels reported here, (j = 6.5, F_1, e), but in the v = 3 vibrational level rather than v = 4. They reported $k_{jj}^{(0)}(expt)$ = (3.74 ± 0.2) x 10^{-10} cm^3 s^{-1} and $k_{jj}^{(0)}(theory)$ = 3.93 x 10^{-10} cm^3 s^{-1}, in excellent agreement with our measurement of $k_{jj}^{(0)}$ = (3.92 ± 0.03) x 10^{-10} cm^3 s^{-1}. Converting $k_{jj}^{(0)}$ to a thermally averaged cross-section, yields $\sigma_{jj}^{(0)} \approx 62$ Å^2 for low j levels, decreasing to 41 Å^2 for j = 23.5. This implies a collision radius of ≈ 4.4 Å for the lowest j. This radius is considerably larger than that defined by the repulsive core of the CN(A)-Ar PESs calculated by Alexander *et al.*[57] but compares favourably to the average range of the attractive well.

We also observe a significant $k_{jj}^{(2)}$ at low-j, typically ≈ 1 x 10^{-10} cm^3 s^{-1}, which falls off as j increases, reaching zero within experimental error at j = 23.5. The mean thermally averaged collision cross-section, $\langle \sigma_{jj}^{(2)} \rangle$, for j =1.5 – 6.5 is 18 Å^2, much smaller than the total elastic cross-section, $\sigma_{j \to j}^{(0)}$, which, based on calculations on the similar NO(X)+Ar system, would be expected to be of the order of 250 Å^2.[38] This indicates clearly that most elastic collisions are not m_j changing.

As discussed in the introduction, measurements of elastic depolarization (Δj = 0, $\Delta m_j \neq 0$) are generally much rarer than those of population loss, and there are no others of $k_{jj}^{(2)}$ for CN with which to compare our results. The older literature on collisional depolarization, inspired by the experiments of McCaffery and co-workers on I_2 and alkali metal dimers colliding with rare gases,[77,78] has tended to create an impression that all elastic depolarizing collisions are very inefficient, leading to effectively no loss of alignment on the timescale of RET. Subsequent experiments on self-collisions of C_2H_2 by Halpern and co-workers indicated that more generally

depolarization can be an efficient process.[39-41] The orientation and alignment elastic depolarization rates were both measured, and found to be essentially equal, and to decline with increasing j. The similar orientation and alignment rate constants are inconsistent with any simple model in which the magnitude of Δm_j in a single collision is restricted, as these will lead to destruction of alignment faster than orientation. More complicated models can lead to predictions of faster orientation than alignment loss, but the only model that predicts equal rate constants for both is one in which elastic collisions can completely randomise the initial m_j distribution. Halpern and co-workers speculated that this was the result of elastic depolarization arising preferentially from collisions out of the rotational plane, whilst j – changing collisions occurred preferentially in plane. We have only measured the alignment depolarization, which on its own does not allow us to distinguish between competing models of this type. However, the observation that $k_{jj}^{(2)}$ declines with increasing j is consistent with the contrary behaviour of there being a restricted range of Δm_j, or the classical picture of a rotor that becomes more difficult to tip as the angular momentum increases.

A significant difference between the current experiments and the earlier work just discussed is the open-shell nature of CN $A^2\Pi$. A more suitable collision system for comparison in this and other regards would be NO($X^2\Pi$)-Ar. This obviously has very similar kinematics, and is also calculated to have a V_{sum} PES of comparable well-depth (≈ 100 cm^{-1}) and similar 'T-shaped' geometry to that of CN(A)-Ar.[79] There are no experimental results for NO(X) + Ar elastic depolarization, but recent quantum scattering calculations predict very modest depolarization of the alignment, with the depolarization cross-section peaking at ≈ 7 $Å^2$ for j = 1.5 and declining rapidly to ≈ 1 $Å^2$ by j = 6.5.[38] Clearly then, comparable V_{sum} PESs and kinematics are not enough in

themselves to enforce similar elastic depolarization behaviour. The kinematically identical system NO(A)-Ar has recently been studied using QBS by Brouard and co-workers.[35] The NO(A)-Ar PES has a well depth of ≈ 100 cm^{-1} with the minimum in a linear geometry.[80] Although their experiments were unable to resolve pure elastic depolarization, closed-shell quantum scattering calculations give $\sigma_{jj}^{(2)}$ = 18 $Å^2$ for the N = 2 state. As they have previously shown, this closed shell depolarization cross-section will be split into pure elastic depolarization and spin-rotation changing components once the Hund's case-(b) nature of NO(A) is taken into consideration, making direct comparison with CN(A) difficult.

Considering other similarities that might be determining factors in elastic depolarization, the kinematically distinct system, OH($X^2\Pi$) + Ar has been studied recently both experimentally by our own group,[15-19] and by quantum scattering calculations.[36,38] Again, the V_{sum} potential is of similar well-depth, but this time the minima are at linear geometries. Experiment and theory agree that elastic depolarization is large for the low j levels ($\sigma_{jj}^{(2)}$ ≈ 20 $Å^2$), resembling CN(A) + Ar, but it also undergoes a dissimilar, much more rapid decline with increasing j, becoming negligible by j = 6.5. A related system that is both kinematically distinct, and has a very different PES, is OH($A^2\Sigma^+$)-Ar, where the well-depth at the global minimum is ≈ 1700 cm^{-1}, and is strongly anisotropic. Elastic depolarization in this case is found to be rapid ($\sigma_{jj}^{(2)}$ ≈ 20 $Å^2$) and to be largely independent of j in the range j = 0.5 – 14.5.[23-25] Although the large low-j cross sections are again reminiscent of CN(A) + Ar, the lack of a significant decline with j is not. It appears that in this more extreme case, the deep, anisotropic, well is able to efficiently depolarize even rapidly rotating OH(A) molecules.

These comparisons on the basis of kinematics and the attractive well-depth of single PESs do not reveal any clear trends or systematic dependences of the elastic depolarization. We have, however, hereto ignored a fundamental property of the collision systems, namely that single PESs are, with the exception of the OH(A)-Ar system, insufficient to describe the scattering dynamics. Taking the example of NO(X)-Ar and OH(X)-Ar, although the V_{sum} potentials for these systems are similar in well-depth, the V_{diff} potentials, which in the Hund's case-(a) limit control spin-orbit changing collisions,[81,82] are considerably different. Dagdigian and Alexander have shown that the V_{diff} potential makes a major contribution to the elastic depolarization for OH(X)+Ar, but makes little or no contribution to that of NO(X)+Ar.[38] This can be attributed to the effective range of their respective V_{diff} PES. For OH(X)-Ar, the V_{diff} PES has a significant magnitude beyond the range of the repulsive wall in the V_{sum} potential, and spin-orbit manifold changing collisions are a significant fraction of the total RET cross-section.[19] In contrast, for NO(X)-Ar, the V_{diff} PES acts at shorter range than the V_{sum} PES.[79] As a result of this, collisions that change spin-orbit manifold have considerably smaller cross-sections than spin-orbit conserving ones for NO(X)-Ar.[83] The V_{diff} PES for CN(A)-Ar, like that of OH(X)-Ar, has a significant magnitude at the range of the V_{sum} attractive minimum, and the cross-sections for spin-orbit changing collisions are similar to those for conserving transitions.[57] We therefore speculate that the V_{diff} potential may well play an important role in the elastic depolarization of CN(A) by Ar. However, a significant additional difference for CN(A) + Ar is the possibility of EET to the $X^2\Sigma^+$ state, mediated by the V_1 coupling PES. Dagdigian and co-workers' experiments on collisions of CN ($A^2\Pi$, v = 3, j = 6.5, F_1, f) with Ar found EET cross-sections to be very similar to those observed for RET within the A state.[75] However, on the reasonable basis that the V_1 coupling

strength was, in contrast, predicted theoretically to be very weak in thermally accessible regions, the V_1 and V_Σ PESs computed in ref [57] were not included in the accompanying scattering calculations of CN(A) + Ar RET rate constants. These nevertheless agreed well with the corresponding experimental relative rate constants.[57] RET is usually assumed to be primarily determined by the repulsive wall of the PES, suggesting that the electrostatic coupling is unimportant in this region. In contrast, elastic depolarization is expected to be sensitive to longer ranges extending into the attractive well.[23,36] As was discussed in the introduction, recent experiment and theory have shown considerably deeper attractive minima in both the V_{sum} and V_Σ surfaces than originally calculated by Alexander and co-workers,[57] which will also have an as yet undetermined effect on the magnitude of the V_1 coupling PES.[50,52] It is therefore an interesting and open question to what extent the V_1 and V_Σ PESs may also contribute to the elastic depolarization of CN(A), which could be addressed by further QM scattering calculations.

5.2 State-to-state rate constants and transferred alignment

The state-to-state population transfer rate constants shown in figure 8, display the almost universal strongly decreasing trend in magnitude with increasing Δj, resulting from energy and linear-to-angular momentum transfer restrictions.[84,85] They also agree well in both absolute magnitude and state-to-state propensities with the quantum scattering calculations by Alexander *et al.* on the *ab-initio* PESs for $v = 3$.[57] Also shown are their experimental results, scaled to theory for transfer to the $J = 4.5$, F_1, e state, with which there is further good agreement. Alexander *et al.* have discussed in some detail the comparison between experiment and theory, which we do not reproduce here. Clearly the change in vibrational level from $v = 3$ to $v = 4$ has little effect on the RET dynamics. However, the agreement between our

measurements and those previously reported gives us confidence in our experimental technique.

Turning to the transferred alignment, there are, as discussed in the introduction, a limited number of previous experimental studies of this property. Two extreme limits may be established, complete retention of polarization, or its complete randomization. The former behaviour was observed in RET of Li_2 and I_2 with rare gases, notably He.[11,12,86] There are obviously strong kinematic reasons for expecting retention of polarization in I_2 + He RET, which might be described as a prototype HH + L system. I_2 + He and Li_2 + He are also examples where essentially only repulsive forces are significant, and the PESs exhibit low anisotropy. At the other limit, recent experiments and theory on OH(A)-Ar have shown that an open-shell PES may result in near total scrambling of polarization in a single collision.[23,25,34] As noted earlier in the discussion, this OH(A)-Ar PES has a deep attractive well, which is highly anisotropic, and provides efficient elastic depolarization for a wide range of initial *j*. Clearly this indicates that the simple picture of polarization retention as a result of purely repulsive forces during RET is not always applicable.

In the experiments reported here we find product alignments that are typically ~ 30-55% of those in the initial level, and hence occupy a middle ground between the two extreme limits. There are no directly comparable experiments on open-shell Π-state species with similar kinematics e.g. NO(X)-Ar. The closest kinematic comparison that is available is the recent study by Brouard and co-workers on the NO(A)-Ar system.[35] They were not able to directly measure state-to-state transfer efficiencies, but they did report the results of classical trajectory calculations. Specifically, they found collisional transfer efficiencies for NO(A) + Ar from the initial $N = 7$ level to be remarkably similar to those reported here for CN, ranging

from ≈ 0.6 for $\Delta N = \pm 1$ transitions, to ≈ 0.35 for $\Delta N = \pm 3$. This closed-shell calculation clearly shows that substantial depolarization can occur during RET on a single PES, which is also consistent with two earlier polarization transfer experiments on closed-shell self-collisions. In the first of these, Sitz and Farrow used an OODR technique to prepare and probe aligned samples of N_2 $^1\Sigma_g^+$ ($v = 1$), and hence to study N_2 self-collisions.[42,43] They observed alignment retention of ≈ 75% in the transfer from $j = 6$ to $j' = 4$, substantially more than observed here for CN(A) + Ar, although as they noted this was also clearly inconsistent with complete retention of m_j. Halpern and co-workers used OODR to study collisional transfer of orientation and alignment in C_2H_2 self-collisions.[39-41] The alignment retention they observed was very similar to that reported here, averaging 40% for a range of $\Delta j = \pm 2$ transitions studied.[39] The simplest models to fit these polarization ratios are ones in which limited ranges of either Δm_j or classical tilt angle, $\theta_{jj'}$, are allowed. With measurements limited to purely one tensor moment of the m_j distribution there will always be a range of parameters in such a model that will fit the data. Measurements of multiple tensor moments, i.e. orientation and alignment, allow some constraints to be applied. However, all such models should be regarded with caution, as without careful design it is easy to create one which is non-physical. For example, a pure $\Delta m_j = 0$ conserving model applied to transfer of an alignment from $j = 1$ to $j = 2$ would create a $K = 4$ moment in the product polarization that cannot be present in the initial distribution.[42] The creation of higher order anisotropic moments in this fashion is of course impossible in an isotropic environment. For this reason, among others, we do not attempt to construct any such models here.

It is possible to convert the measured alignment transfer efficiency into an average classical tilt angle, $\theta_{jj'}$.[34]

$$\frac{\Gamma^{(2)}_{j\to j'}}{\Gamma^{(0)}_{j\to j'}} = \left\langle P_2\left(\cos\theta_{jj'}\right)\right\rangle \qquad (20)$$

The highest observed efficiency in CN(A) + Ar is for the Δj = -1 transfer, where we measure $\left\langle P_2\left(\cos\theta_{jj'}\right)\right\rangle = 0.55 \pm 0.06$, giving a classical tilt angle, $\theta_{jj'}$ = (33 ± 3)°, whilst the lowest efficiency for the Δj = +3 transition $\left\langle P_2\left(\cos\theta_{jj'}\right)\right\rangle = 0.32 \pm 0.08$ gives $\theta_{jj'}$ = (42 ± 3)°. These classical angles emphasise that a substantial change in the direction of j is observed here, implying that the magnitude of the orbital angular momentum transferred in the collision is significant compared to the relatively low rotational angular momentum. A simple vector picture gives the resulting transferred orbital angular momentum, $|l| = |\mathbf{j} - \mathbf{j}'| \approx 4$ ħ for Δj = -1 and $|l| \approx 6$ ħ for Δj = +3. Whilst these are indeed similar in magnitude to the rotational angular momenta, they are small compared to the absolute magnitude of the orbital angular momenta. Taking an impact parameter of 3.8Å, corresponding to the attractive minimum of the V_{sum} PES, and the average thermal relative collision speed for CN + Ar, we find $|l| \approx 60$ ħ. The transferred orbital angular momentum is thus consistent with a small **k**,**k'** scattering angle, i.e. strong forward scattering, as has been previously observed for small Δj transitions in CN(A) + Ar.[59]

This analysis might encourage the interpretation of the polarization transfer data within a simple classical scattering model, in which the small Δj transitions observed result from forward scattering at large impact parameter on the attractive parts of the V_{sum} PES, with the relative magnitudes of orbital and rotational angular momenta resulting in substantial depolarization for even relatively modest torques. However, as discussed above in the context of the elastic depolarization, the assumption that the V_{sum} PES alone is responsible for the depolarization may not be a good one. There are no QM scattering calculations for polarization transfer available

for the CN(A)-Ar system. However, there are some related calculations on NO(X)-Ar by Orlikowski and Alexander.[73] They showed that significant alignment depolarization was possible for RET between the lowest few levels in the system. Interestingly, they also showed that strong alternations in the polarization transfer efficiency as a function of rotational state and parity were possible. As is apparent in figure 10, we see no such variation, which if present would appear as an alternating preference for conservation of alignment in the *e/f* Λ-doublets as a function of *j'*. There are, though, substantial differences between the experiments reported here and the NO(X) + Ar calculations, not least in the magnitude of the *j* and *j'* studied. It is thus far from clear whether such an alternation should really be expected for the initial level studied here for CN(A) + Ar. Further QM scattering calculations on the available *ab-initio* PESs for CN(A,X)-Ar would therefore clearly be very useful. These would enable the exploration of the relative contributions to the polarization transfer efficiency of the V_{sum} and V_{diff} PESs, together with those of the V_{Σ} PES and V_1 coupling PES, as well as addressing the open question of parity-dependent propensities.

6. Conclusions

We have measured the collisional removal and transfer of both population and alignment on a state-resolved level for the CN($A^2\Pi$, $v = 4$) + Ar system. The total population removal rate constants for different initial rotational states, and the state-to-state population transfer rate constants, are in excellent agreement with previous QM scattering calculations on *ab-initio* PESs.[57] The rate constants for elastic depolarization of rotational alignment are significant at low-*j*, falling effectively to zero by $j = 23.5$. Alignment transfer efficiency measurements on RET from the $j = 6.5$ initial state to a variety of product states also show substantial loss of polarization.

These observations add to the growing body of experimental and theoretical evidence that collisional depolarization in elastic and inelastic collisions can be a rapid process, in contrast to models based on purely repulsive intermolecular interactions. Comparison to the limited body of similar measurements and theory on the related OH(X,A)-Ar and NO(X)-Ar systems suggests that the open-shell nature of the CN may play a significant role in the collisional depolarization. In particular, we suggest that QM scattering calculations to determine the relative contributions of the V_{sum} and V_{diff} PESs, and the extent of influence of the V_{Σ} PES and V_{1} coupling PES, would be valuable in furthering the understanding of conservation and destruction of rotational angular momentum polarization in elastic and inelastic collisions.

Acknowledgements

We thank Prof. P. J. Dagdigian for the communication of the state-to-state rate constants included in figure 8. We thank the Research Councils U.K. for an Academic Fellowship for M.L.C. and the Leverhulme Trust for a project grant.

References

1 A. Schiffman and D. W. Chandler, Int Rev Phys Chem **14**, 371 (1995).
2 J. C. Whitehead, Rep Prog Phys **59**, 993 (1996).
3 P. J. Dagdigian, Annu Rev Phys Chem **48**, 95 (1997).
4 J. J. Gilijamse, S. Hoekstra, S. Y. T. van de Meerakker, G. C. Groenenboom, and G. Meijer, Science **313**, 1617 (2006).
5 A. J. McCaffery, M. J. Proctor, and B. J. Whitaker, Annu Rev Phys Chem **37**, 223 (1986).
6 M. L. Costen, S. Marinakis, and K. G. McKendrick, Chem Soc Rev **37**, 732 (2008).
7 K. T. Lorenz, D. W. Chandler, J. W. Barr, W. W. Chen, G. L. Barnes, and J. I. Cline, Science **293**, 2063 (2001).
8 E. A. Wade, K. T. Lorenz, D. W. Chandler, J. W. Barr, G. L. Barnes, and J. I. Cline, Chem Phys **301**, 261 (2004).
9 R. N. Zare, *Angular Momentum: Understanding Spatial Aspects in Chemistry and Physics*. (Wiley, New York, 1988).
10 K. Blum, *Density Matrix Theory and Applications*, 2nd ed. (Plenum Press, New York, 1996).
11 H. Kato, S. R. Jeyes, A. J. McCaffery, and M. D. Rowe, Chem Phys Lett **39**, 573 (1976).
12 M. D. Rowe and A. J. McCaffery, Chem Phys **43**, 35 (1979).
13 V. Khare, D. J. Kouri, and D. K. Hoffman, J Chem Phys **74**, 2275 (1981).
14 T. Orlikowski and M. H. Alexander, J Chem Phys **80**, 4133 (1984).
15 H. J. Crichton, M. L. Costen, and K. G. McKendrick, J Chem Phys **119**, 9461 (2003).
16 M. L. Costen, H. J. Crichton, and K. G. McKendrick, J Chem Phys **120**, 7910 (2004).
17 S. Marinakis, G. Paterson, J. Kłos, M. L. Costen, and K. G. McKendrick, Phys Chem Chem Phys **9**, 4414 (2007).
18 S. Marinakis, G. Paterson, G. Richmond, M. Rockingham, M. L. Costen, and K. G. McKendrick, J Chem Phys **128**, 021101 (2008).
19 G. Paterson, S. Marinakis, M. L. Costen, K. G. McKendrick, J. Kłos, and R. Toboła, J Chem Phys **129**, 074304 (2008).
20 G. Paterson, S. Marinakis, M. L. Costen, and K. G. McKendrick, Phys Scripta **80** (2009).
21 G. Paterson, S. Marinakis, J. Klos, M. L. Costen, and K. G. McKendrick, Phys Chem Chem Phys **11**, 8804 (2009).
22 G. Paterson, S. Marinakis, M. L. Costen, and K. G. McKendrick, Phys Chem Chem Phys **11**, 8813 (2009).
23 M. L. Costen, R. Livingstone, K. G. McKendrick, G. Paterson, M. Brouard, H. Chadwick, Y.-P. Chang, C. J. Eyles, F. J. Aoiz, and J. Kłos, J Phys Chem A, In Press (2009).
24 M. Brouard, A. Bryant, I. Burak, S. Marinakis, F. Quadrini, I. A. Garcia, and C. Vallance, Mol Phys **103**, 1693 (2005).
25 M. Brouard, A. Bryant, Y. P. Chang, R. Cireasa, C. J. Eyles, A. M. Green, S. Marinakis, F. J. Aoiz, and J. Kłos, J Chem Phys **130**, 044306 (2009).
26 E. A. Brinkman and D. R. Crosley, J Phys Chem A **108**, 8084 (2004).
27 S. Williams, L. A. Rahn, and R. N. Zare, J Chem Phys **104**, 3947 (1996).

[28] A. Brockhinke, W. Kreutner, U. Rahmann, K. Kohse-Höinghaus, T. B. Settersten, and M. A. Linne, Appl Phys B-Lasers O **69**, 477 (1999).

[29] T. B. Settersten, R. L. Farrow, and J. A. Gray, Chem Phys Lett **369**, 584 (2003).

[30] X. L. Chen, B. D. Patterson, and T. B. Settersten, Chem Phys Lett **388**, 358 (2004).

[31] X. L. Chen and T. B. Settersten, Appl Optics **46**, 3911 (2007).

[32] M. L. Costen and K. G. McKendrick, J Chem Phys **122**, 164309 (2005).

[33] G. Paterson, S. Marinakis, M. L. Costen, K. G. McKendrick, J. Kłos, and R. Toboła, J Chem Phys, In Press (2009).

[34] F. J. Aoiz, M. Brouard, C. J. Eyles, J. Kłos, and M. P. de Miranda, J Chem Phys **130**, 044305 (2009).

[35] M. Brouard, H. Chadwick, Y. P. Chang, R. Cireasa, C. J. Eyles, A. O. La Via, N. Screen, F. J. Aoiz, and J. Kłos, J Chem Phys **131**, 104307 (2009).

[36] P. J. Dagdigian and M. H. Alexander, J Chem Phys **130**, 094303 (2009).

[37] P. J. Dagdigian and M. H. Alexander, J Chem Phys **130**, 164315 (2009).

[38] P. J. Dagdigian and M. H. Alexander, J Chem Phys **130**, 204304 (2009).

[39] J. B. Halpern, R. Dopheide, and H. Zacharias, J Phys Chem-Us **99**, 13611 (1995).

[40] A. D. Rudert, J. Martin, W. B. Gao, J. B. Halpern, and H. Zacharias, J Chem Phys **111**, 9549 (1999).

[41] A. D. Rudert, J. Martin, W. B. Gao, H. Zacharias, and J. B. Halpern, J Chem Phys **112**, 9749 (2000).

[42] G. O. Sitz and R. L. Farrow, J Chem Phys **101**, 4682 (1994).

[43] G. O. Sitz and R. L. Farrow, J Chem Phys **103**, 489 (1995).

[44] R. Fei, H. M. Lambert, T. Carrington, S. V. Filseth, C. M. Sadowski, and C. H. Dugan, J Chem Phys **100**, 1190 (1994).

[45] J. Z. Guo, C. M. Sadowski, Q. Gao, and F. J. Morgan, J Chem Phys **113**, 7276 (2000).

[46] S. M. K. Brunet, J. Z. Guo, T. Carrington, S. V. Filseth, and C. M. Sadowski, J Chem Phys **116**, 3617 (2002).

[47] K. M. Hickson, C. M. Sadowski, and I. W. M. Smith, Chem Phys Lett **372**, 443 (2003).

[48] R. V. Olkhov and I. W. M. Smith, Phys Chem Chem Phys **8**, 5643 (2006).

[49] R. V. Olkhov and I. W. M. Smith, J Chem Phys **126**, 134314 (2007).

[50] J. D. Han, M. C. Heaven, U. Schnupf, and M. H. Alexander, J Chem Phys **128**, 224309 (2008).

[51] A. Khachatrian, P. J. Dagdigian, D. I. G. Bennett, F. Lique, J. Kłos, and M. H. Alexander, J Phys Chem A **113**, 3922 (2009).

[52] J. Han, M. C. Heaven, and U. Schnupf, J Chem Phys **128**, 224309 (2008).

[53] X. Yang, P. J. Dagdigian, and M. H. Alexander, J Chem Phys **112**, 4474 (2000).

[54] B. Nizamov, P. J. Dagdigian, and M. H. Alexander, J Chem Phys **115**, 8393 (2001).

[55] B. Nizamov, P. J. Dagdigian, Y. R. Tzeng, and M. H. Alexander, J Chem Phys **115**, 800 (2001).

[56] B. Nizamov, X. Yang, P. J. Dagdigian, and M. H. Alexander, J Phys Chem A **106**, 8345 (2002).

[57] M. H. Alexander, X. Yang, P. J. Dagdigian, A. Berning, and H. J. Werner, J Chem Phys **112**, 781 (2000).

58 A. Alagappan, I. Ballingall, M. L. Costen, K. G. McKendrick, and G. Paterson, Phys Chem Chem Phys **9**, 747 (2007).
59 A. Alagappan, I. Ballingall, M. L. Costen, and K. G. McKendrick, J Chem Phys **126**, 041103 (2007).
60 G. E. Hall and S. W. North, Annu Rev Phys Chem **51**, 243 (2000).
61 A. Alagappan, M. L. Costen, and K. G. McKendrick, Spectrochimica Acta Part a-Molecular and Biomolecular Spectroscopy **63**, 910 (2006).
62 M. L. Costen, S. W. North, and G. E. Hall, J Chem Phys **111**, 6735 (1999).
63 I. Nadler, D. Mahgerefteh, H. Reisler, and C. Wittig, J Chem Phys **82**, 3885 (1985).
64 M. L. Costen and G. E. Hall, Phys Chem Chem Phys **9**, 272 (2007).
65 R. N. Dixon, J Chem Phys **85**, 1866 (1986).
66 G. E. Hall and M. Wu, J Phys Chem **97**, 10911 (1993).
67 M. L. Costen and G. E. Hall, Phys Chem Chem Phys **7**, 1408 (2005).
68 M. L. Hause, G. E. Hall, and T. J. Sears, J Mol Spectrosc **253**, 122 (2009).
69 S. W. North, X. S. Zheng, R. Fei, and G. E. Hall, J Chem Phys **104**, 2129 (1996).
70 B. Follmeg, P. Rosmus, and H. J. Werner, J Chem Phys **93**, 4687 (1990).
71 A. J. Alexander, J Chem Phys **123** (2005).
72 A. J. Orr-Ewing and R. N. Zare, Annu Rev Phys Chem **45**, 315 (1994).
73 M. H. Alexander and T. Orlikowski, J Chem Phys **80**, 1506 (1984).
74 Y. H. Huang, R. C. Lu, and J. B. Halpern, Appl Optics **32**, 981 (1993).
75 J. H. Guo, A. Ali, and P. J. Dagdigian, J Chem Phys **85**, 7098 (1986).
76 L. Rubio-Lago, D. Sofikitis, A. Koubenakis, and T. P. Rakitzis, Phys Rev A **74** (2006).
77 M. D. Rowe and A. J. McCaffery, Chem Phys **34**, 81 (1978).
78 J. McCormack, A. J. McCaffery, and M. D. Rowe, Chem Phys **48**, 121 (1980).
79 M. H. Alexander, J Chem Phys **111**, 7426 (1999).
80 J. Klos, M. H. Alexander, R. Hernandez-Lamoneda, and T. G. Wright, J Chem Phys **129** (2008).
81 M. H. Alexander, J Chem Phys **76**, 5974 (1982).
82 G. C. Corey and M. H. Alexander, J Chem Phys **85**, 5652 (1986).
83 A. Lin, S. Antonova, A. P. Tsakotellis, and G. C. McBane, J Phys Chem A **103**, 1198 (1999).
84 A. J. McCaffery, Z. T. Alwahabi, M. A. Osborne, and C. J. Williams, J Chem Phys **98**, 4586 (1993).
85 M. A. Osborne and A. J. McCaffery, J Chem Phys **101**, 5604 (1994).
86 S. R. Jeyes, A. J. McCaffery, and M. D. Rowe, Mol Phys **36**, 1865 (1978).

Figure 1. Integrated Doppler line intensities as a function of time, $I_{\parallel}$ (filled circles) and $I_{\perp}$ (open circles) for the CN $A^2\Pi$ ($v = 4$, $j = 2.5$, F_1, e) state colliding with Ar (200 mTorr), probed on the A-X(4,2) $R_1(1.5)$ transition.

Figure 2. FM Doppler profiles for the CN $A^2\Pi$ ($v = 4$, F_1, $j = 2.5$, e) state, pumped via the A-X(4,0) $R_1(1.5)$ transition and probed via the A-X(4,2) $R_1(1.5)$ transition. Signal averaged over a 10 ns gate at the peak of the pump pulse. (a) Parallel geometry and (b) perpendicular geometry. In each case, the filled circles represent stimulated emission and the open circles dispersion. The solid lines are the results of fitting all 4 profiles simultaneously to Gaussian lineshapes with relative intensities determined by a population and a rotational alignment, as described in the text.

Figure 3. Loss of population (circles) and alignment (squares) for the CN $A^2\Pi$ ($v = 4$, F_1, $j = 2.5$, e) state, at a total pressure of 200 mTorr (open) and 1000 mTorr (filled), as a function of delay from the pump laser pulse. The solid lines are single exponential fits to the data.

Figure 4. Rates for population (circles) and alignment (squares) loss as a function of Ar number density for $j = 2.5$ (filled) and $j = 13.5$ (open). Lines are linear fits to determine the 2nd-order rate constants.

Figure 5. Second-order rate constants for loss of population, $k_{jj}^{(0)}$, (open circles) and alignment, $k_{jj}^{(2)}$, (filled circles) as a function of j. The errors are 2σ from the linear fits to the second-order plots.

Figure 6. FM Doppler profiles for the CN $A^2\Pi$ ($v = 4$, F_1, $j' = 9.5$, f) state probed via the A-X(4,2) $Q_1(9.5)$+$^Q R_{12}(8.5)$ transition, resulting from RET from the $A^2\Pi$ ($v = 4$, F_1, $j = 6.5$, e) level pumped via the A-X(4,0) $R_1(5.5)$ transition. Signal averaged over a 10 ns gate starting 75 ns after the pump pulse. (a) Parallel geometry and (b) perpendicular geometry. In each case, the filled circles represent stimulated emission and the open circles dispersion. The solid lines are the results of fitting all 4 profiles simultaneously to sums of Gaussian lineshapes with relative intensities determined by rotational alignment sensitivity and main/sub-branch rotational linestrengths, as described in the text.

Figure 7. Population, $A_0^{(0)}$, as a function of post-pump delay time at a total pressure of 400 mTorr. Filled circles, initially prepared level ($j = 6.5$, F_1, e). Open circles $\Delta j = +1$, Λ-conserving ($j' = 7.5$, F_1, e). Open squares $\Delta j = +2$, Λ-conserving ($j' = 8.5$, F_1, e). Open triangles $\Delta j = -2$, Λ-conserving ($j' = 4.5$, F_1, e). The transferred populations have been multiplied by 20 to put them on the same scale as the initial level, the solid lines are fits to a single exponential decay or the kinetic scheme described in the text, as appropriate.

Figure 8. State-to-state population transfer rate constants, $k_{j\to j'}^{(0)}$, from ($j = 6.5$, F_1, e) as a function of Δj within the F_1 spin-orbit manifold. Filled symbols, Λ-doublet conserving transitions, open symbols, Λ-doublet changing transitions. Circles, this work, triangles and squares are experimental and theoretical results respectively, from ref. [57].

Figure 9. Alignment, $A_0^{(2)}$, as a function of post-pump delay, at a total pressure of 400 mTorr. Filled circles, initially prepared level ($j = 6.5$, F_1, e). Open circles, $\Delta j = +1$, Λ-conserving ($j' = 7.5$, F_1, e). Open squares, $\Delta j = +2$, Λ-conserving ($j' = 8.5$, F_1, e). The solid lines are fits to single exponential decays, as described in the text.

Figure 10. Ratio of state-to-state alignment to population transfer rates, $\Gamma^{(2)}_{j\to j'}/\Gamma^{(0)}_{j\to j'}$ from ($j = 6.5$, F_1, e) as a function of Δj within the F_1 spin-orbit manifold. Filled symbols, Λ-doublet conserving transitions, open symbols, Λ-doublet changing transitions.

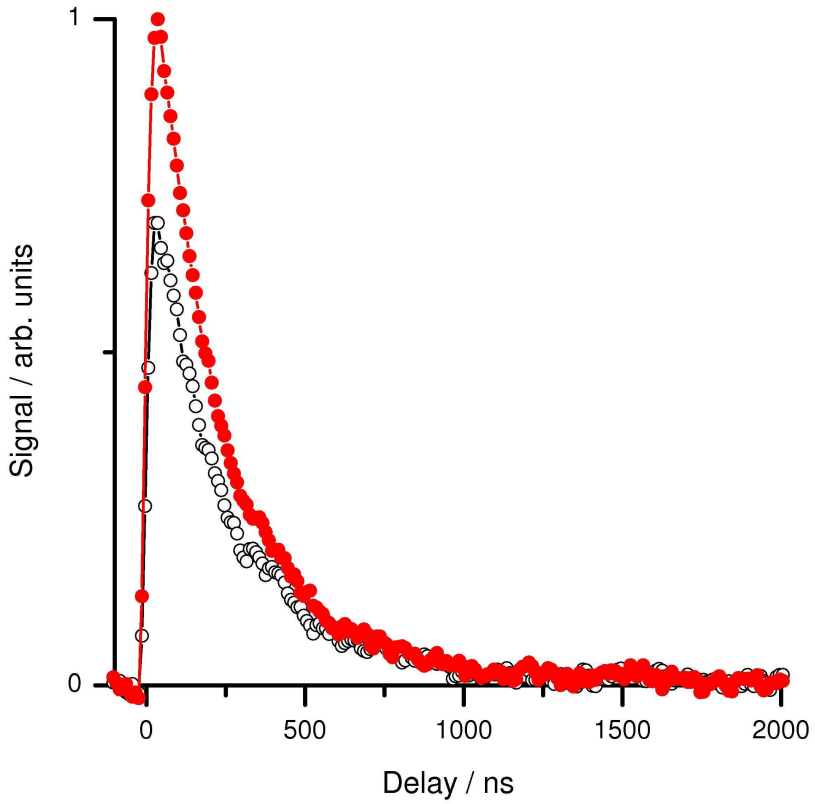

Figure 1
120x130mm (600 x 600 DPI)

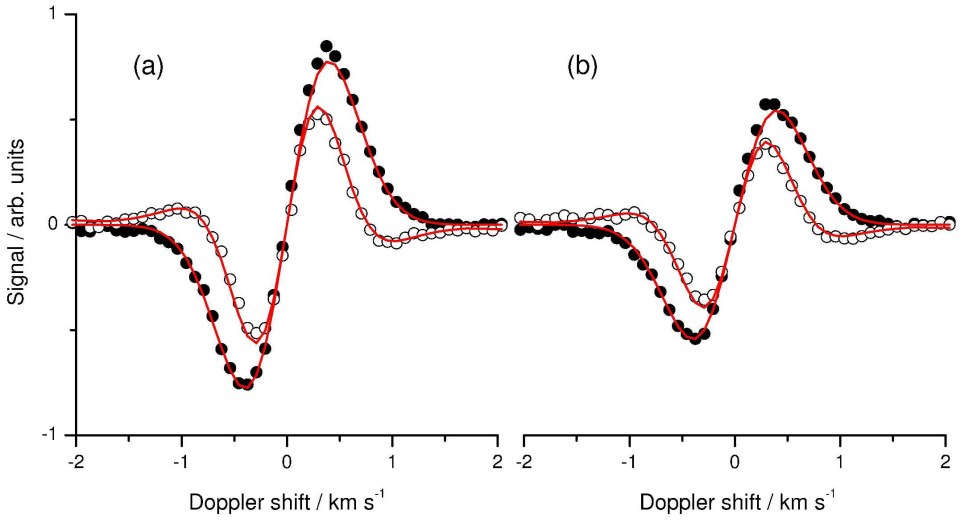

Figure 2
190x120mm (600 x 600 DPI)

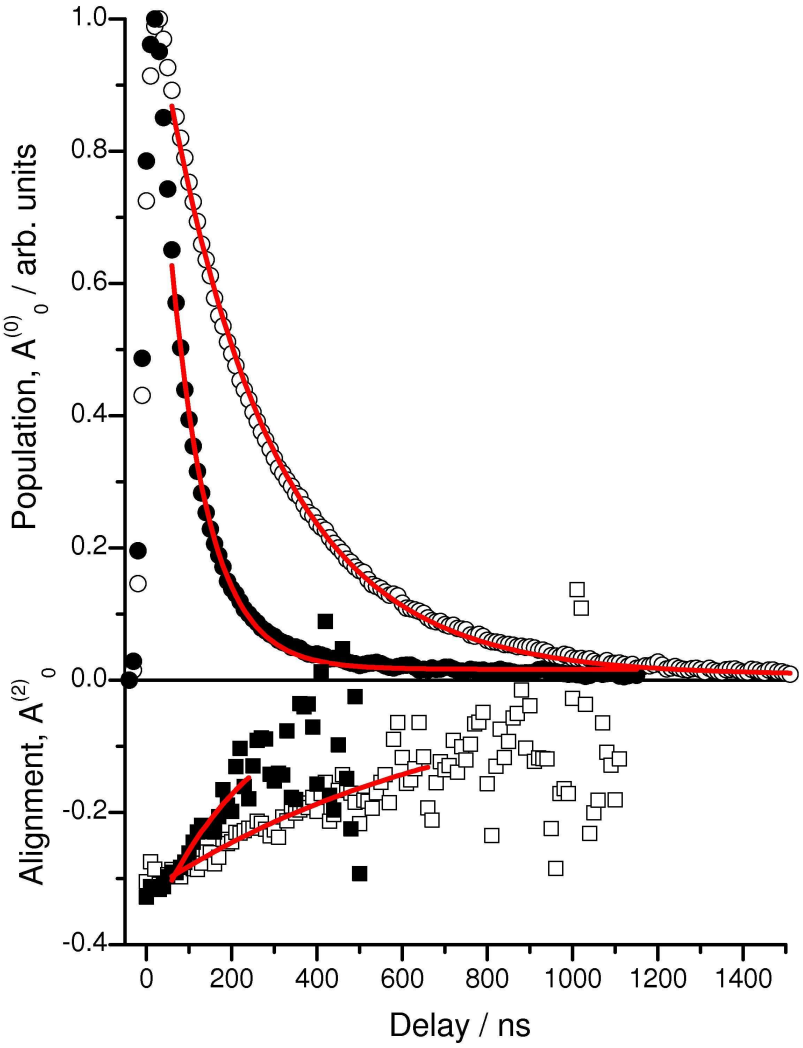

Figure 3
110x145mm (600 x 600 DPI)

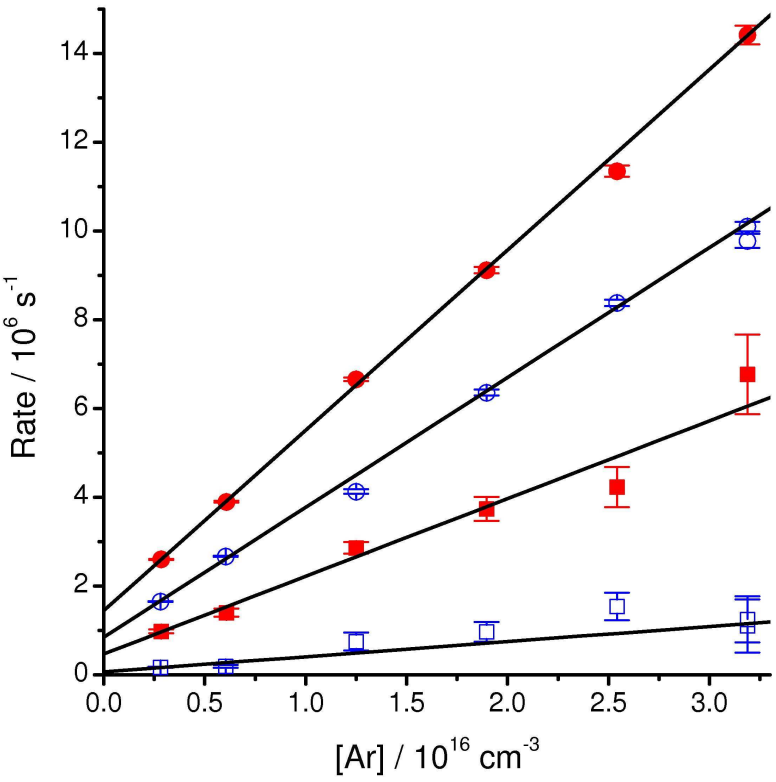

Figure 4
120x115mm (600 x 600 DPI)

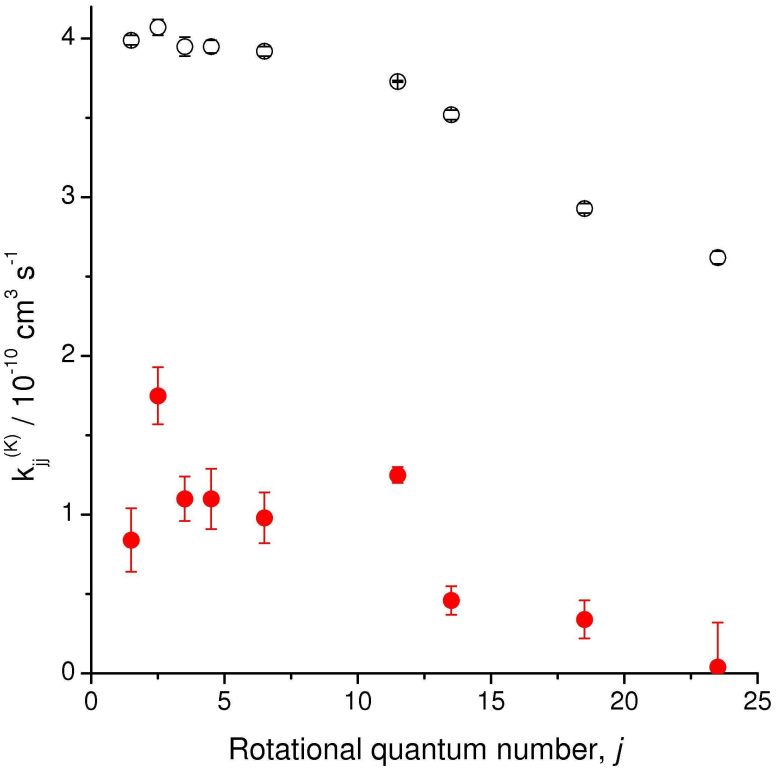

Figure 5
120x110mm (600 x 600 DPI)

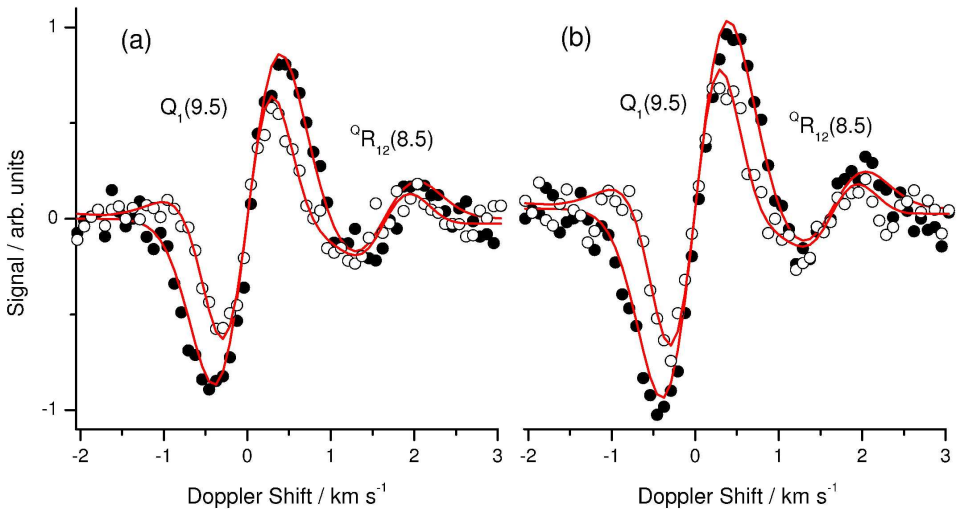

Figure 6
190x120mm (600 x 600 DPI)

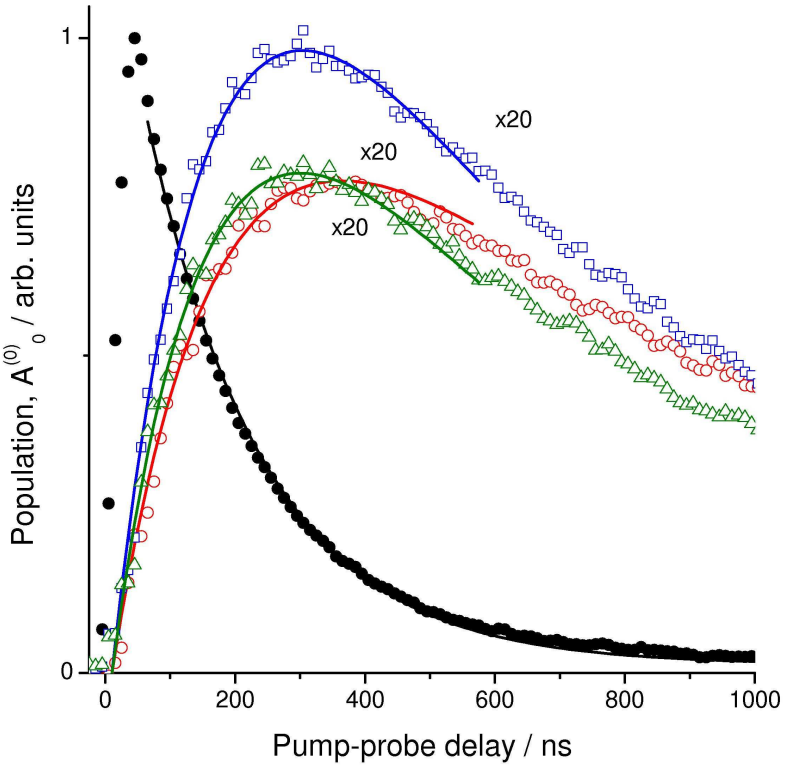

Figure 7
120x110mm (600 x 600 DPI)

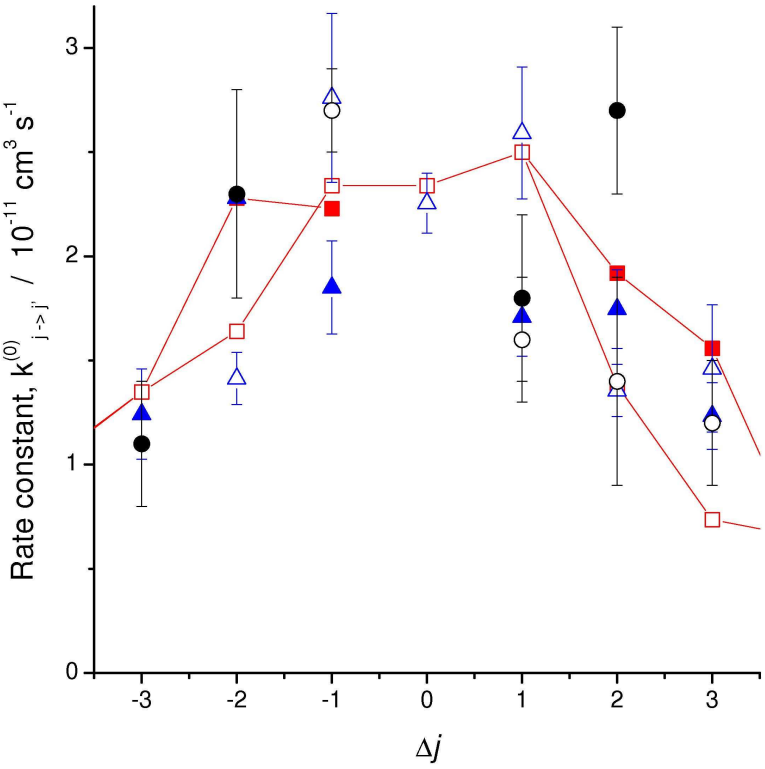

Figure 8
120x110mm (600 x 600 DPI)

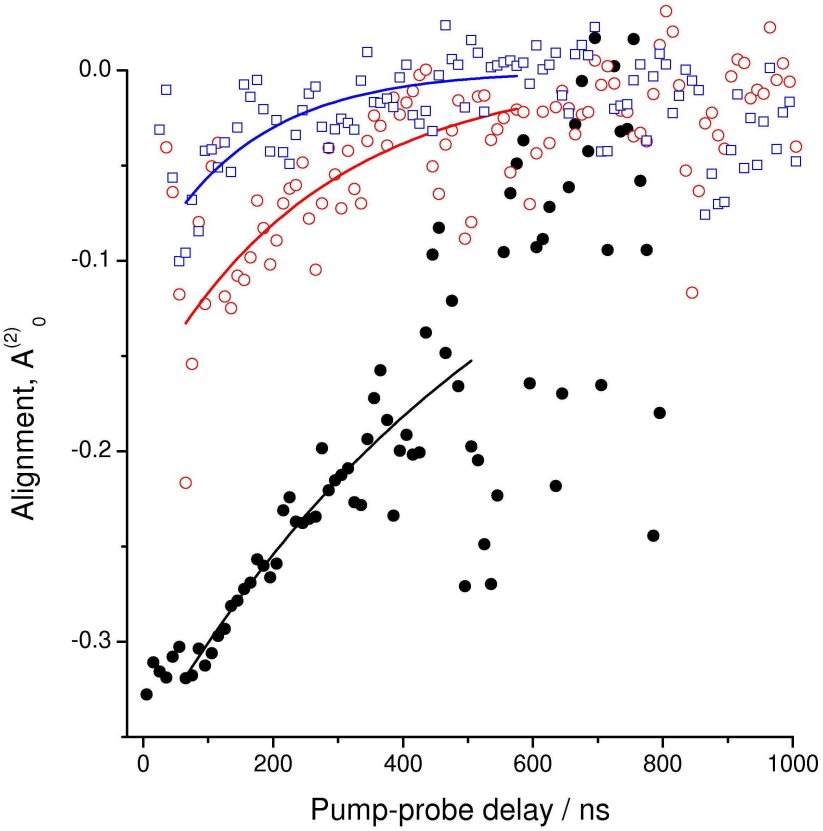

Figure 9
120x110mm (600 x 600 DPI)

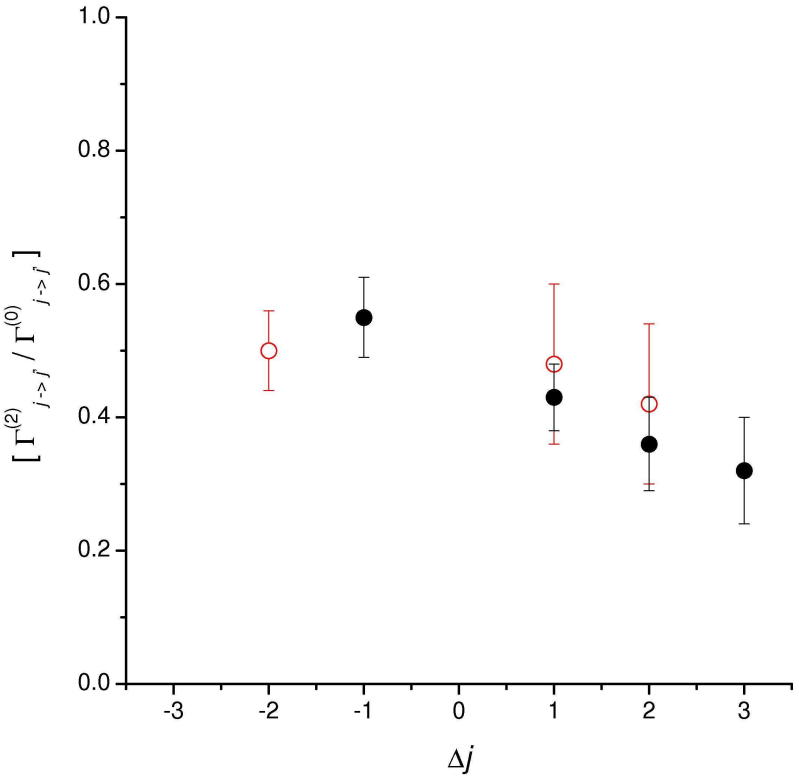

Figure 10
120x110mm (600 x 600 DPI)